

SAR Compliance Simulation Report for iPhones

Model No.	FCC ID
A2650	BCG - E8140A
A2889	BCG - E8150A
A2890	BCG - E8151A
A2891	BCG - E8152A
A2892	
A2651	BCG - E8141A
A2893	BCG - E8154A
A2894	BCG - E8155A
A2895	BCG - E8156A
A2896	

Date of Simulation:

04/11/2022-06/09/2022

Location:

Apple Inc., Cupertino, CA, USA

Table of Contents

1	Introduction.....	5
2	Wireless Power Transfer System.....	6
3	SAR Simulations Methodology.....	7
4	H-field Simulations for Transmitter	8
5	SAR Simulations	10
5.1	Exposure Cases:	13
5.2	Additional Exposure Cases:	16
6	Impact of Housing Size.....	19
7	Summary.....	22
	Annex A: Specific information for SAR computational modelling.....	23

List of Figures:

Figure 1: Model validation workflow for computational exposure assessment.	7
Figure 2: H-field measurement setup for Tx only	8
Figure 3: Simulation Vs Measured H-field comparison for direct exposure case	9
Figure 4: Initial mesh generation and then refinement through adaptive meshing technique in HFSS.	12
Figure 5: Spatial 1-gram average SAR for Case 202 (b), (a) full view, (b) side view.	15
Figure 6: Spatial 1-gram average SAR for Case 1 (a), (a) full view, (b) side view.....	17
Figure 7: Peak E-field distribution inside Phantom for Direct Exposure Case 1(a)	18
Figure 8: Comparison of 2022 iPhone Dimensions for A2650, A2889, A2890,A2891, A2892 and A2651, A2893, A2894, A2895, A2896	19
Figure 9: Waveguide filled half with vacuum and half with dielectric	25
Figure 10: Dipole Antenna Model	26
Figure 11: Toroid Model.....	28
Figure 12: Current loop in front of a cuboid	29
Figure 13: Current Density plot	30
Figure 14: IEEE P1528.4 for SAR computation.....	31

List of Tables:

Table 1. Key design parameters	6
Table 2: Averaged 1-g SAR and Peak Spatial Average E-field (inside Phantom) simulation results for the nominal use cases	14
Table 3. Averaged 1-g SAR and Peak Spatial Average E-field (inside Phantom) simulation results for direct exposure cases	16
Table 4. Comparison of Average SAR and Peak Spatial Average E-field for different housing sizes	20
Table 5. Peak Spatial Average SAR (W/Kg) plots for different housing sizes	21
Table 6: Criteria for the waveguide evaluation.....	24
Table 7: Reflection at a dielectric interface	26
Table 8: Simulated Dipole parameters.....	27
Table 9: Budget of uncertainty contributions of the numerical algorithm (filled based on IEC 62704-4 ED1).....	31
Table 10: Uncertainty of DUT Model	32
Table 11: Expanded Standard Uncertainty	32
Table 12: Material Properties and Tolerances	33

1 Introduction

This report demonstrates RF exposure compliance using SAR simulation for 2022 iPhone models (FCC IDs: BCG-E8140A, BCG-E8150A, BCG-E8151A, BCG-E8152A, BCG-E8141A, BCG-E8154A, BCG-E8155A, BCG-E8156A). In addition to being charged by a desktop WPT charger, 2022 iPhone models also support WPT charging function at 360 kHz to charge accessories. Currently, the only accessory that can be charged by iPhones is an Apple accessory: MagSafe Battery Pack. This report presents the evaluation of SAR and E-field induced inside a human tissue when the Phone is wirelessly charging a potential external accessory.

To demonstrate RF exposure compliance for 2022 iPhones at 360 kHz operating frequency, as permitted by §2.1093 (certification for portable devices below 4 MHz), SAR numerical simulations are performed to demonstrate compliance to the 1.6 W/kg localized 1-g SAR limit.

The charging session only occurs when the phone is connected to an AC power outlet. However, due to the potential apple accessory in future and the phone being held in place by magnets, it is envisioned that customers may use the charging function in a portable use condition, for example, charging the battery while making a call or texting. Therefore, to be conservative we evaluate iPhone WPT transmitter as a mixed mobile/portable device. Future designs and accessories may support true portable use condition, with the host-client pair able to be placed in a pocket or backpack. In those cases, a body-worn exposure assessment would be conducted.

The following sections describe the modeling, measured H-field, simulated H-field, and simulated SAR.

2 Wireless Power Transfer System

The wireless power transfer system consists of a transmitting coil with 13 turns and measures 9.06 uH nominally in free air. The receiver coil consists of 11 turns and measures 7.5 uH nominally in free air. Both coils are wound spirally and made of stranded wire. Below are the details of the Phone (Tx) coil which is used in all the iPhone models described in section 1 of the report.

Tx Coil Winding Type	Spiral, 1 Layer, Stranded Wire
Turns	13
Inner Radius	10.06 mm
Outer Radius	21.35 mm
Cross-section	Rectangular
Thickness	0.13 mm
Width	0.62 mm

Rx Coil Winding Type	Spiral, 1 Layer, Stranded Wire
Turns	11
Inner Radius	10.9 mm
Outer Radius	18.9 mm
Cross-section	Rectangular
Thickness	0.32 mm
Width	0.49 mm

Below are some key initial parameters used in the design that will be helpful in determining worst-case use for exposure: These are common to all the iPhone models described in section 1 of this report.

Table 1. Key design parameters

Item	Description
Max Power Delivered	5 Watt
Functional On-body max offset	Refer to the graph below*
Operating Frequency	$f_0 = 360 \text{ kHz}$
Communications/Modulation Method	FSK -> Phone to Accessory ASK -> Accessory to Phone
Object Detection Mode	Magnetic + NFC

* Refer to antenna location file for all antennas in the phone, and how the WPT coil is separated from other antennas.

3 SAR Simulations Methodology

The following steps has been taken to show the validity of the model used for SAR Simulations:

- 1) EM Simulation:
 - a. Import a CAD model that represents the actual product in the simulation tool.
 - b. Define material properties inside the product based on vendor's inputs.
 - c. Extract two-port network impedance matrix ($[Z]$) from the simulation.
- 2) Circuit Simulation:
 - a. Include the impedance matrix in the wireless power transfer (WPT) circuit model.
 - b. Run circuit simulation and extract coils' current waveforms.
- 3) Field Calculations:
 - a. Use the current waveforms to drive the EM simulation model.
 - b. Calculate H-field from the simulation.
- 4) Validate Simulation Model:
 - a. Measure H-field, and compare with simulation result
 - b. Perform full uncertainty analysis
 - c. Once a correlation is established, and model's accuracy is verified, this model will be used for computational exposure assessments (e.g., SAR simulations).

The entire workflow is summarized and shown in Fig. 1.

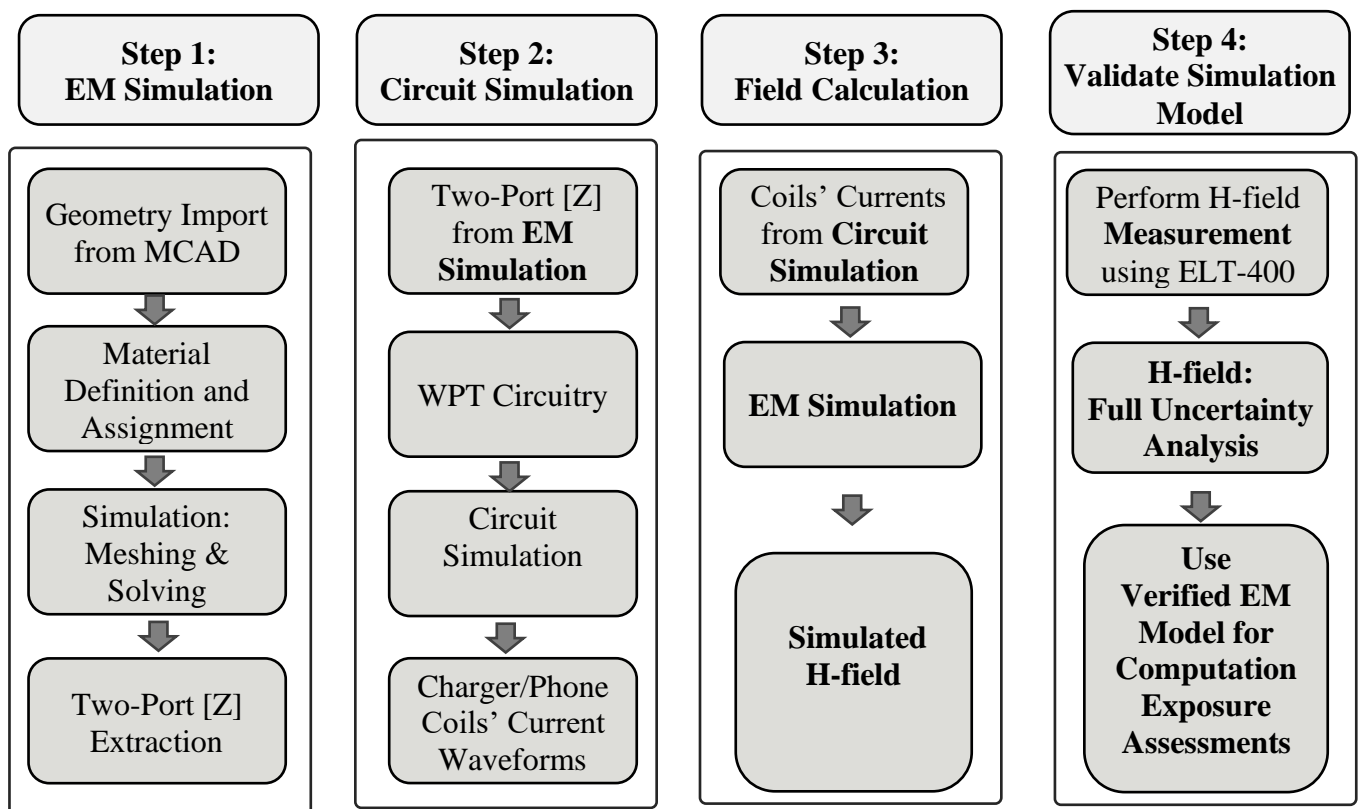


Figure 1: Model validation workflow for computational exposure assessment.

4 H-field Simulations for Transmitter

The Electromagnetics simulations are conducted using commercially available software ANSYS HFSS. To validate the simulation model, H-field measurements are made on the EUT (as explained above) and compared to the simulated model results. The validated model is then used for SAR simulations.

For this study, simulation vs measurement correlation is done for transmitter only scenario. The measurement setup is shown in Fig. 6. As shown in the measurement setup, the center of probe coils is 16mm away from the true 0mm touch position. Following procedure was used to compute the averaged fields from simulation results for correlating with measured data: The volumetric H-field is exported from HFSS and post-processed using a Matlab script to include the ELT400 probe averaging effect. The ELT400 probe has three rotated internal loops (oriented in 3 different angles). These loops measure H-field by integrating it over their effective aperture area. The script will apply this integration over the exported volumetric H-field. It is worth mentioning that the script does not consider any potential loading effect that the probe may have on the DUT, including mutual interaction with the DUT coils. To our experience, this mutual interaction is partially responsible for the discrepancy between the simulation and measurement results when the probe is touching the DUT.

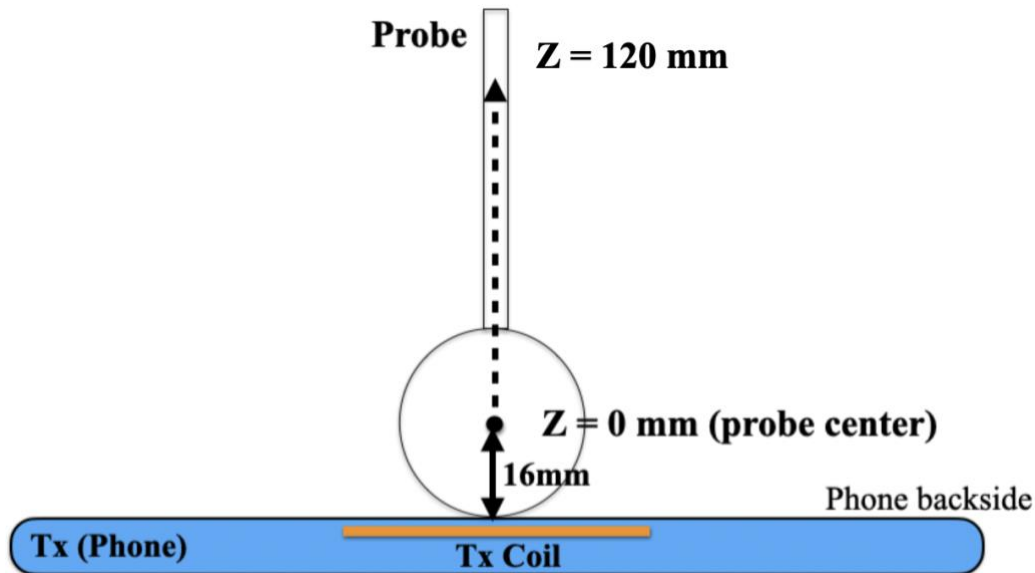


Figure 2: H-field measurement setup for Tx only

Simulation model and measurements correlation is performed at a vertical distance away from the DUT and the probe is moved vertically in Z direction from 0mm (probe center) to 120mm until we reach the noise floor of the measurement probe.

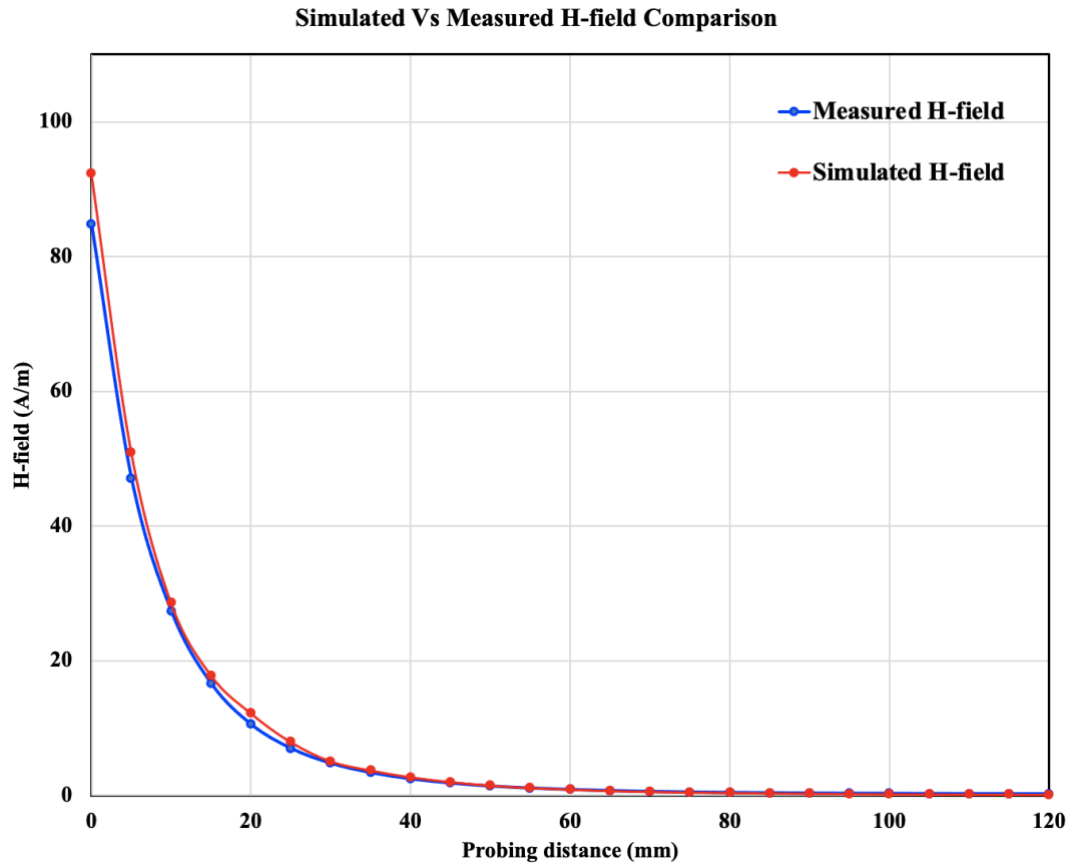


Figure 3: Simulation Vs Measured H-field comparison for direct exposure case

The above Fig. 7 shows good correlation between the measurements and simulations. At distance very close to the DUT, simulations are little more conservative than measurements. This validated simulation model is then used for SAR simulations in the next sections.

5 SAR Simulations

The validated simulation model is used for SAR calculations with a phantom added in contact with the EUT. The simulations are computed on a 96 core CPU server with an available RAM of 4 Terabytes. For this simulation, the model run takes approximately 8 hours to complete.

The following steps are used for accurate SAR calculations:

- 1) Elliptical phantom used in body exposure measurements is commercially available from SPEAG: Outer Dimensions of 600mm x 400mm x 150mm.
- 2) Homogeneous tissue material is used as liquid for desired frequency.
- 3) Power loss in phantom is calculated.
- 4) Divide power loss by mass density to calculate SAR.

$$SAR = \frac{P_l}{\rho}$$

P_l = Power loss density

ρ = Mass density

- 5) Point SAR is averaged over 1g or 10g tissue.
- 6) For SAR simulations, mass density of 1000 Kg/m³ is used for the Phantom.

Human Tissue Material Properties at 360 kHz:

The worst-case scenario has been identified to be when a user is holding the device in hand and taking a call or holding the phone on their body while charging. The electrical properties for body and hand layers are shown below. Since the SAR phantom is homogenous, using the layers' properties, the worst-case scenario is selected and applied for the phantom properties. Therefore, for the SAR simulations, the phantom that has conductivity of 0.5 and permittivity of 5016 at the 360 kHz operating frequency is used.

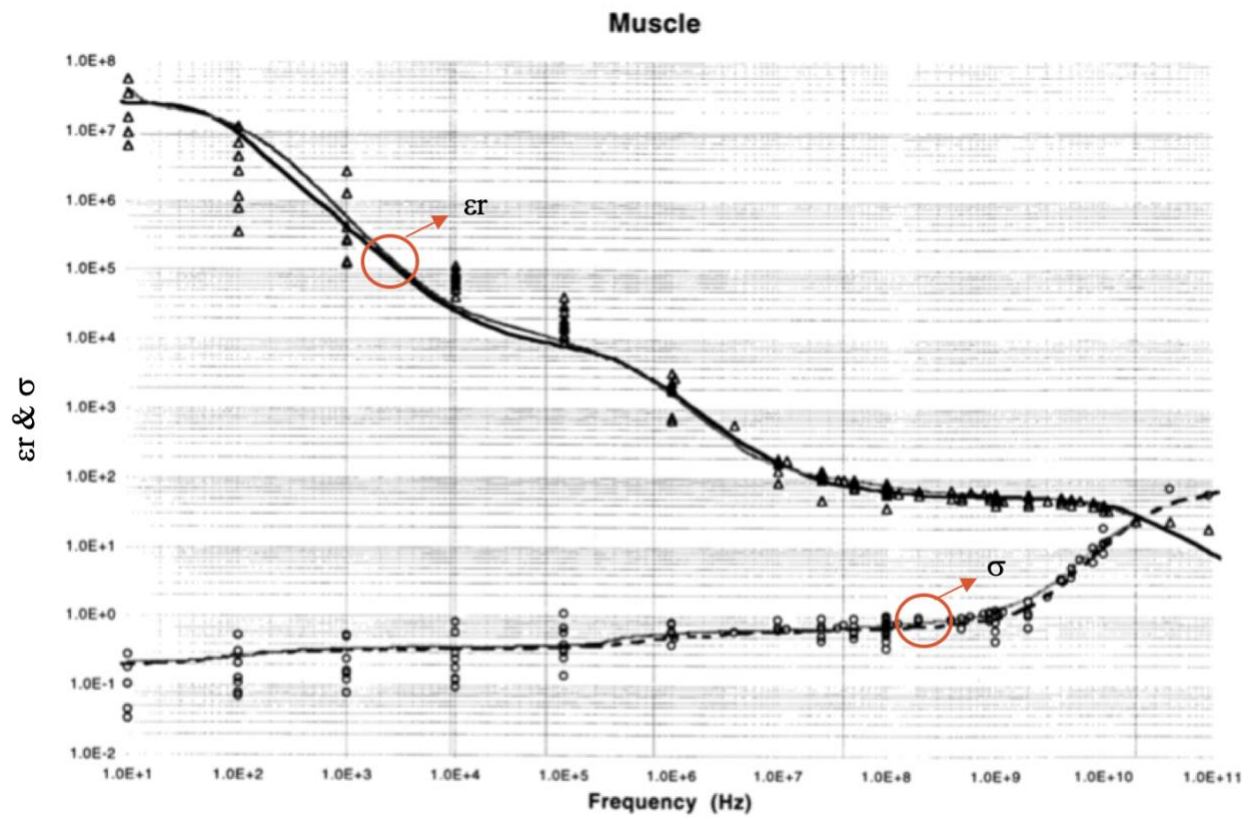
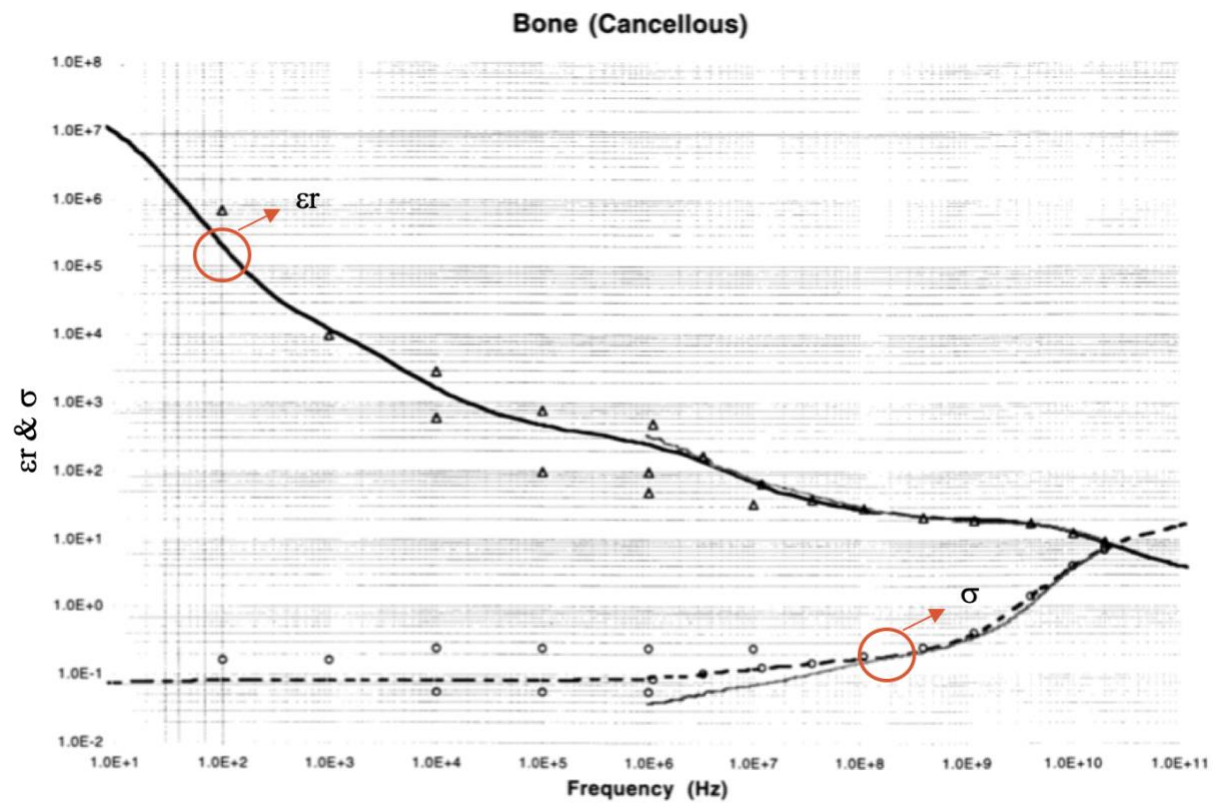
Electrical Properties:

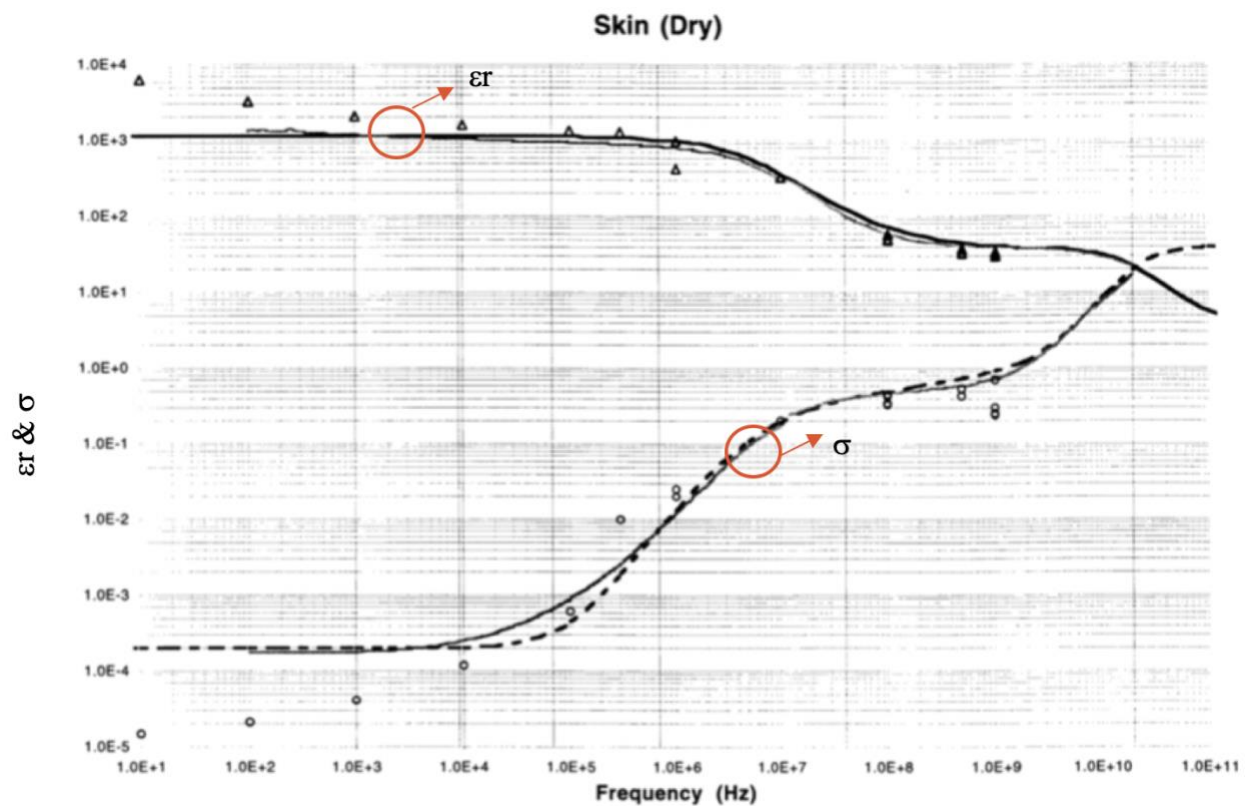
Based on our research this is what we recommend for ϵ_r and sigma (σ) values for body layers

Tissue	Thickness (mm)	Permittivity	Conductivity (S/m)
Skin	3	5016	0.16
Muscle	9	4666	0.5
Bone	20	1414	0.165
Worst case	100	5016	0.5

Based on our research this is what we recommend for ϵ_r and sigma values for hand layers

Tissue	Thickness (mm)	Permittivity	Conductivity (S/m)
Skin	2	5016	0.16
Muscle	2	4666	0.5
Bone	15	1414	0.165
Worst case	100	5016	0.5





Mesh Adaptation:

HFSS adapts the mesh based on field strength. It is important to ensure the mesh is refined to capture SAR accurately. This can be done by using adaptive meshing available in HFSS and mesh refinement process is described in Fig. 8

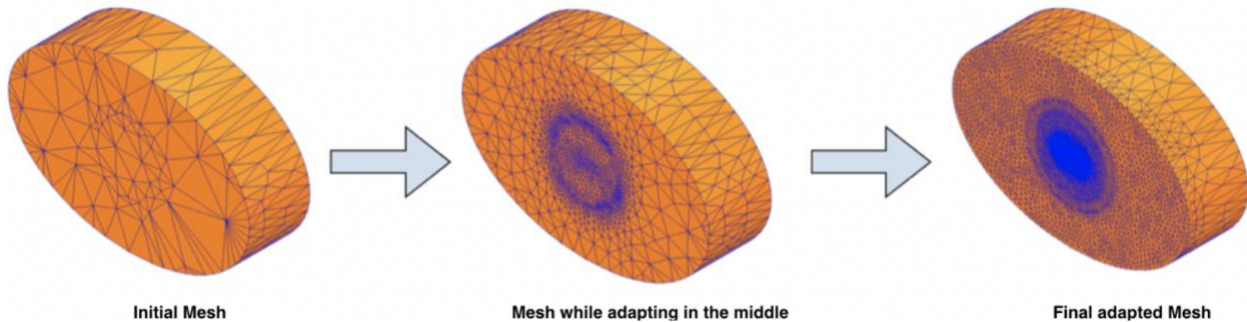


Figure 4: Initial mesh generation and then refinement through adaptive meshing technique in HFSS.

SAR Results:

Using the H-field simulation and measurement tables, two exposure cases were selected for SAR investigation. Considering that the phantom can be in contact with the phone or accessory, there is a total of four scenarios.

5.1 Exposure Cases:

Exposure Case 000 (a): Nominal configuration with perfect alignment and phantom placed above the transmitting unit.

Exposure Case 000(b): Nominal configuration with perfect alignment and phantom placed below the receiving unit.

Exposure Case 202 (a): Misaligned configuration with the worst-case alignment and phantom placed above the transmitting unit.

Exposure Case 202 (b): Misaligned configuration with the worst-case alignment and phantom placed below the receiving unit.

For all the exposure cases, dielectric properties (conductivity and permittivity) used for the phantoms are fixed as (permittivity: 5016, conductivity: 0.5).

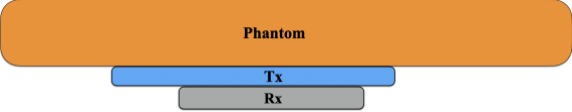
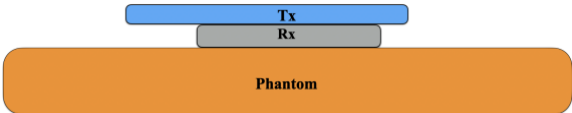
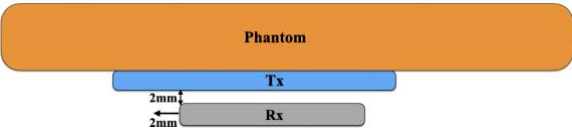
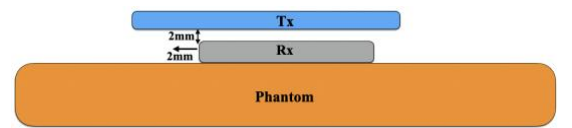
The coil properties are also fixed, transmitting coil with 13 turns and measures 9.06 uH nominally in free air. The receiver coil consists of 11 turns and measures 7.5 uH nominally in free air. Both coils are wound spirally.

The following outputs are calculated and reported in the Table:

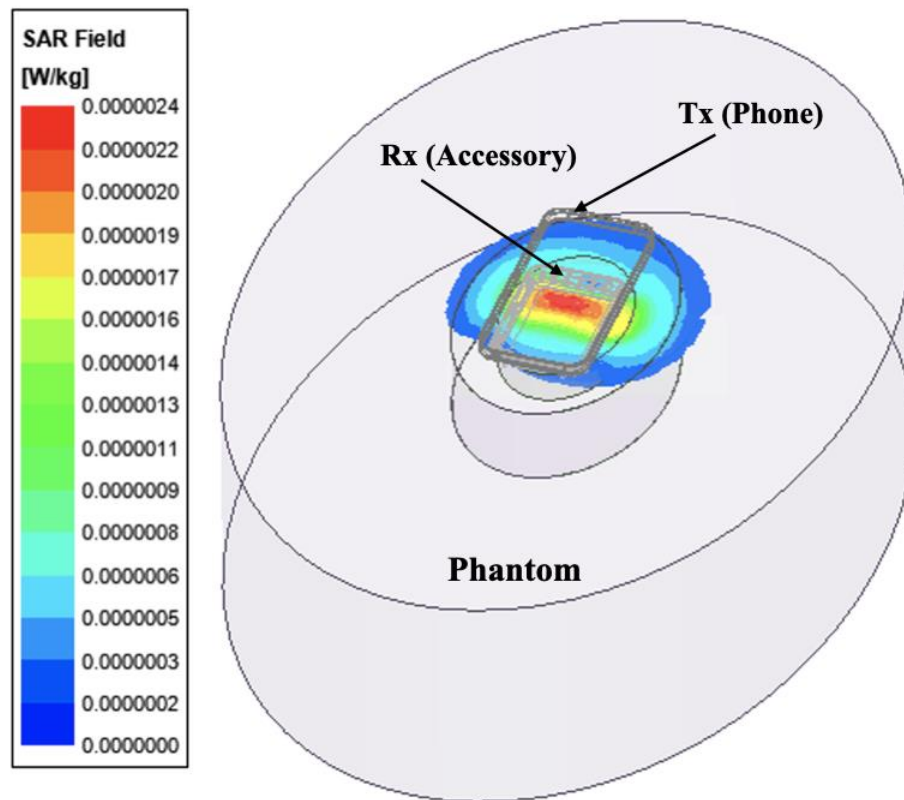
- a. Peak spatial 1-g average SAR in tissue.
- b. Peak spatially averaged electric field in tissue. Electric field is spatially averaged in a contiguous tissue volume of 2 mm by 2 mm by 2 mm.

The simulation results for the use cases and direct exposure scenarios are listed in the Table 6 below:

Table 2: Averaged 1-g SAR and Peak Spatial Average E-field (inside Phantom) simulation results for the nominal use cases.

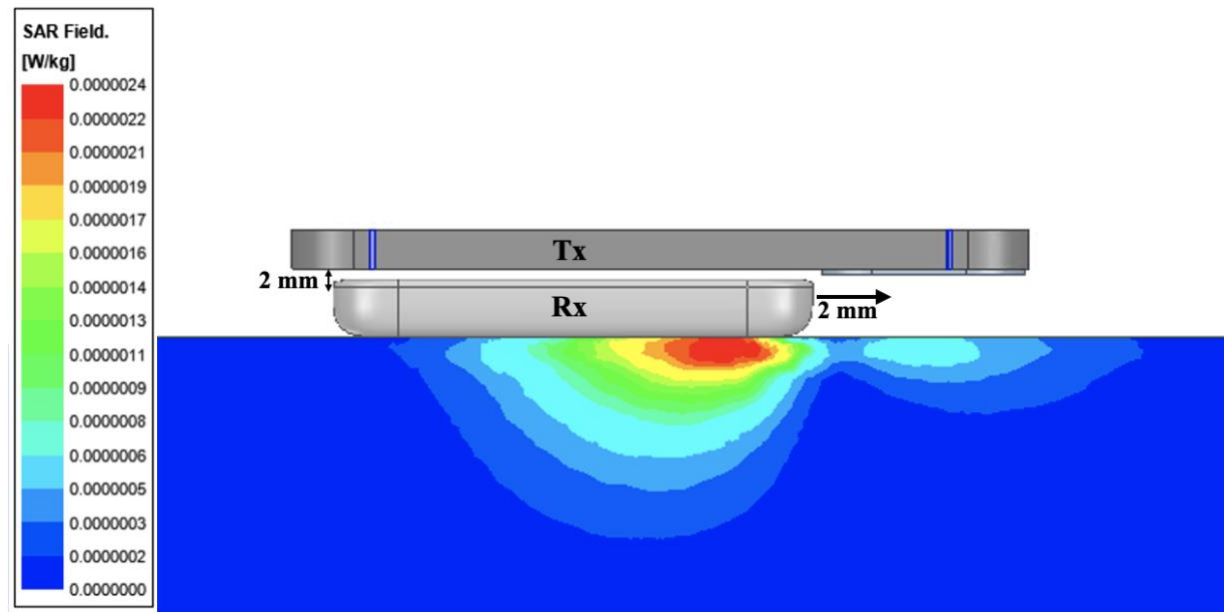
Exposure Case	Description	Peak Spatial Average SAR (W/Kg) Averaged over 1 gram	Peak Spatial Average E-field (V/m) Averaged over 2x2x2 mm ³
Case 000 (a)		0.00000011	0.01
Case 000 (b)		0.00000014	0.017
Case 202 (a)		0.00000020	0.03
Case 202 (b)		0.00000024	0.123

SAR plot is shown in Fig. 9 (a) for Case202(b). The peak spatial 1-g average SAR is 0.0000024 W/kg.



(a) Full view of average SAR plot for Case 202 (b)

The side view is also presented as shown in Fig. 14 (b) below.



(b) Side view of average SAR plot for Case 202 (b)

Figure 5: Spatial 1-gram average SAR for Case 202 (b), (a) full view, (b) side view.

5.2 Additional Exposure Cases:

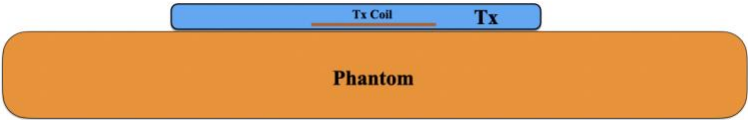
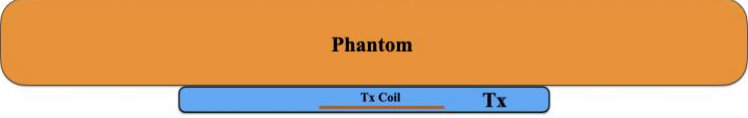
In addition, two corner cases were also investigated that are not likely to happen in normal application when the Phone (Tx) is in direct contact with the Phantom with no accessory present is also investigated.

Direct Exposure (unrealistic) Case 1(a): with receiver absent and the phantom facing towards the phone (Tx) coil.

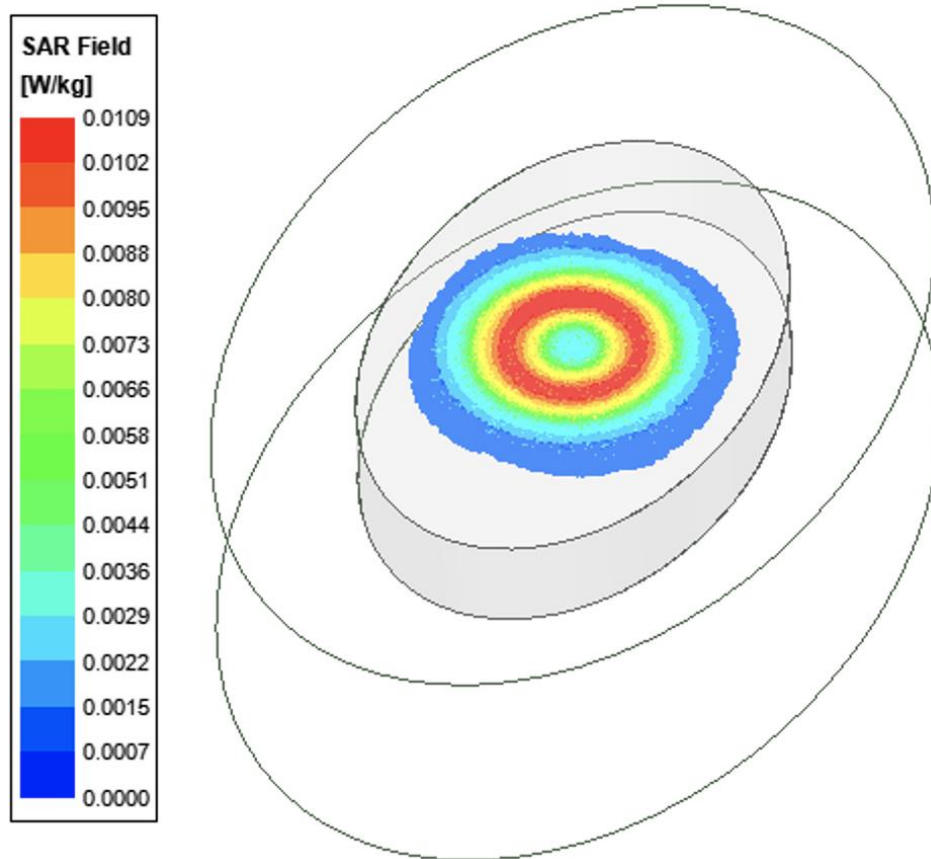
Direct Exposure (unrealistic) Case 1(b): with receiver absent and the phantom facing away from the phone (Tx) coil.

Peak 1-g averaged SAR and E-field inside the Phantom for the Direct exposure cases are shown below.

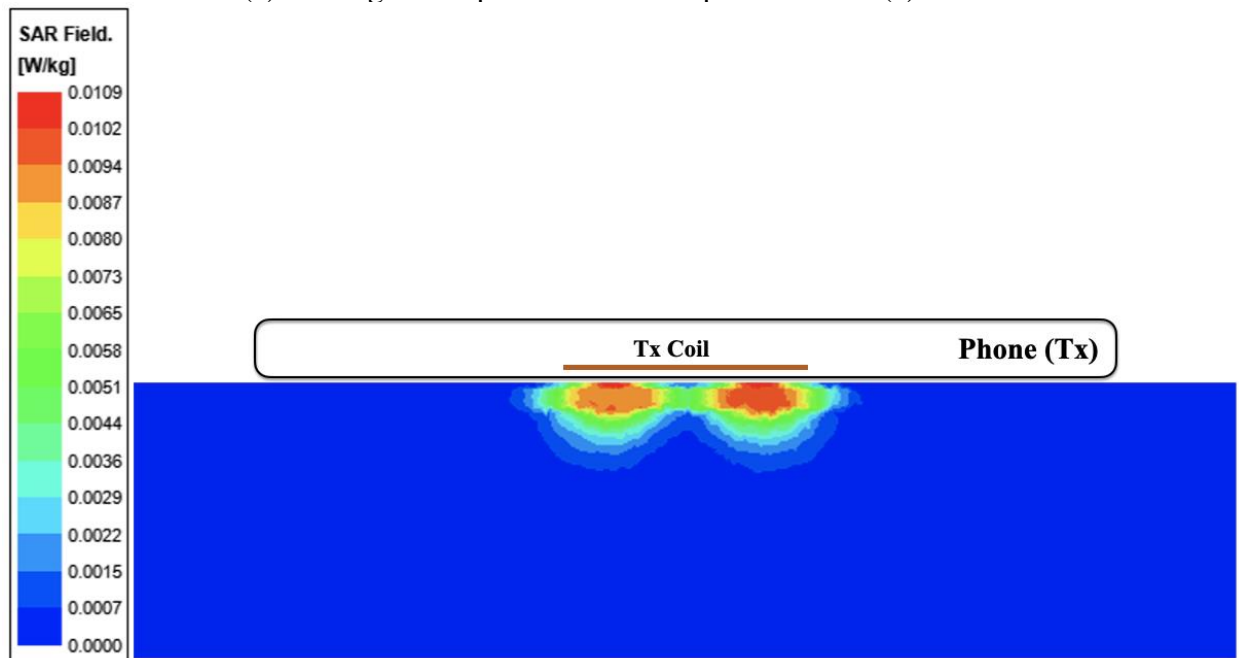
Table 3. Averaged 1-g SAR and Peak Spatial Average E-field (inside Phantom) simulation results for direct exposure cases

Exposure Case	Description	Peak Spatial Average SAR (W/Kg) Averaged over 1 gram	Peak Spatial Average E-field (V/m) Averaged over 2x2x2 mm ³
Case 1(a)		0.011	10.73
Case 1(b)		0.000001	0.1

SAR plot is shown in Fig. 10 for Direct Exposure (unrealistic) Case 1(a). The peak spatial 1-g average SAR is 0.011 W/kg.



(a) Average SAR plot for Direct Exposure Case 1(a)



(b) Side view of average SAR plot for Direct Exposure Case 1(a)

Figure 6: Spatial 1-gram average SAR for Case 1 (a), (a) full view, (b) side view

E-field distribution inside the phantom for the Case1(a) is shown below. Please note that the value reported in the table above was averaged over a cube of 2mmx2mmx2mm and that explains why the value is lower than the peak E-field in this plot.

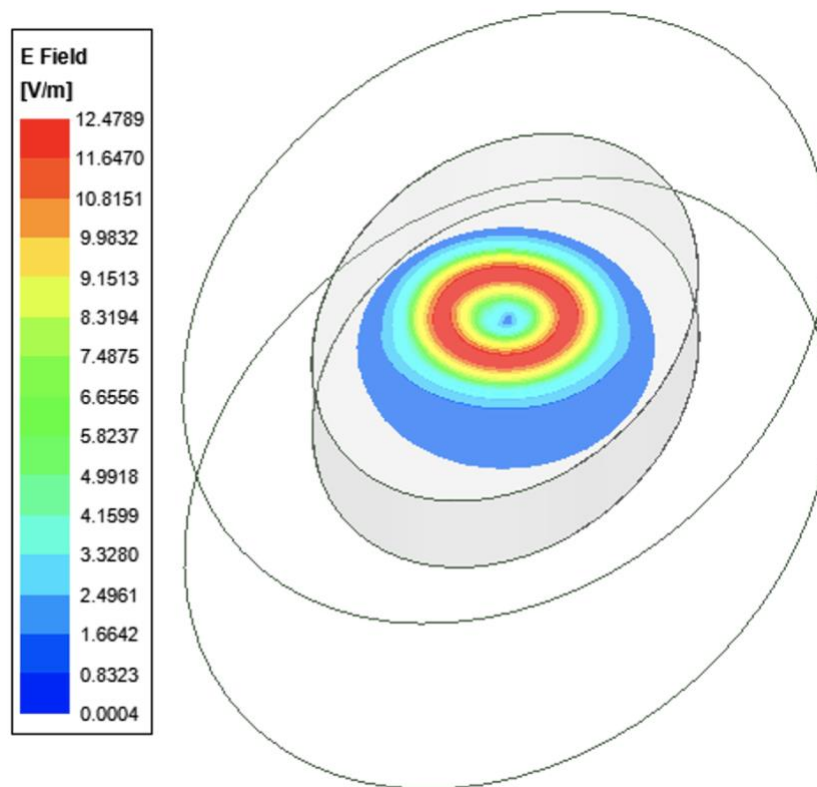


Figure 7: Peak E-field distribution inside Phantom for Direct Exposure Case 1(a)

6 Impact of Housing Size

The phones for 2022 will have two different sizes as summarized in the sketched outlines below. Model No.s, FCC IDs: A2650, BCG-E8140A; A2889, BCG-E8150A; A2890, BCG-E8151A; A2891/A2892, BCG-E8152A on which the detailed analysis was performed in the earlier sections have lower-size dimensions. The larger form factor is for the following Phones: Model No.s, FCC IDs - A2651, BCG-E8141A; A2893, BCG-E8154A; A2894, BCG-E8155A; A2895/A2896, BCG-E8156A.

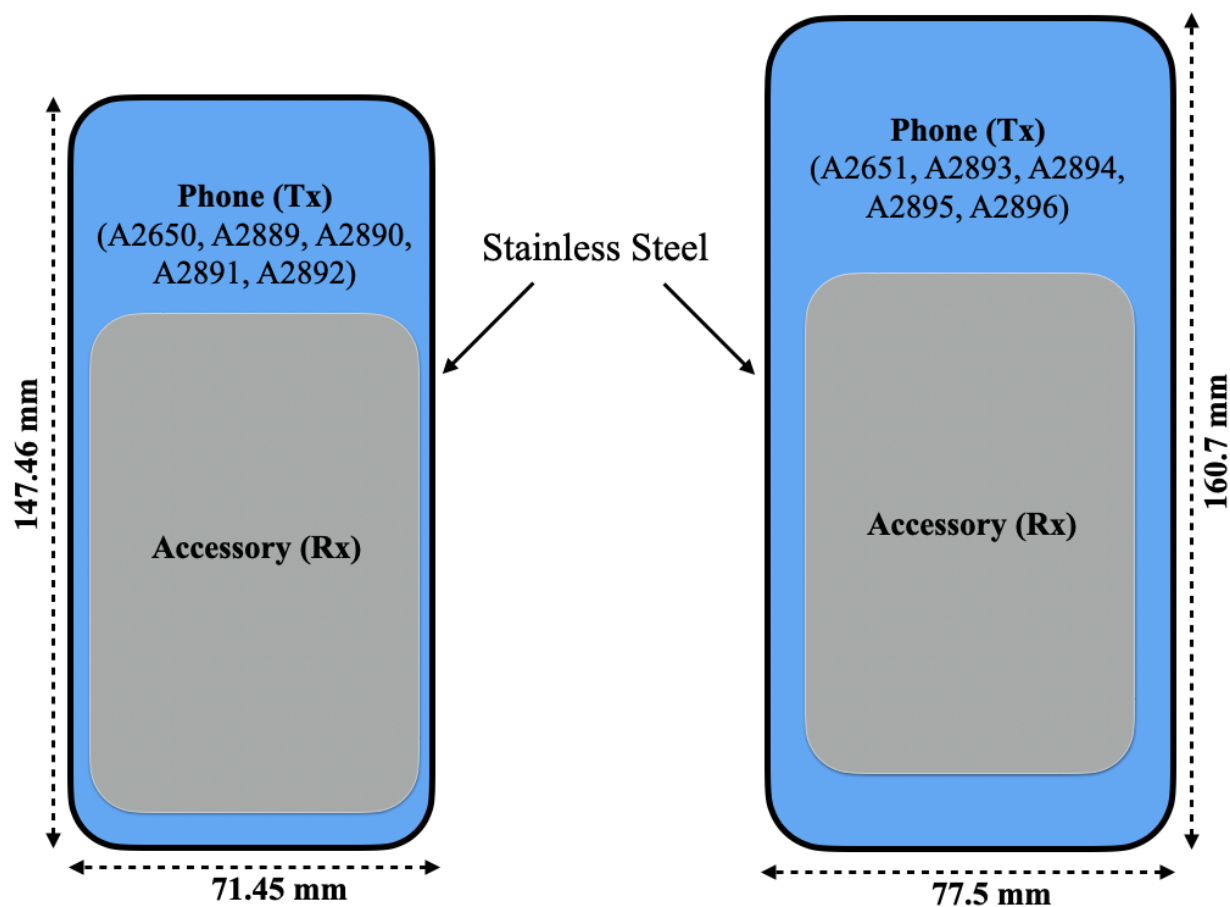


Figure 8: Comparison of 2022 iPhone Dimensions for A2650, A2889, A2890, A2891, A2892 and A2651, A2893, A2894, A2895, A2896

They share common material for the back of the phone and same material (Stainless Steel) is used for housing as well. In this section, we used the worst-case orientation (202-b) from the initial analysis done; to study how the SAR and E-field changes with different housing sizes.

The table below summarizes the results, and the SAR plots are shown for each size.

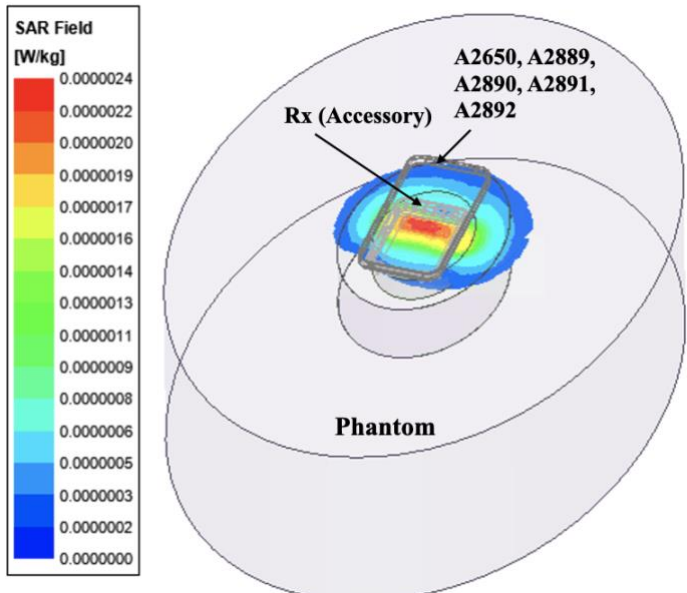
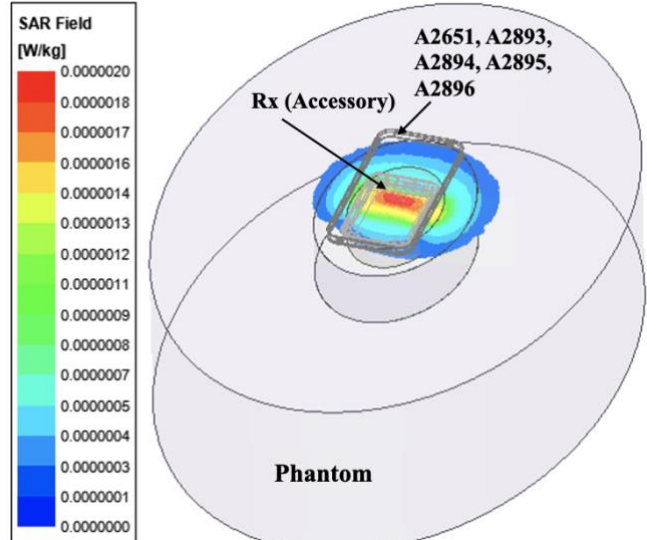
Table 4. Comparison of Average SAR and Peak Spatial Average E-field for different housing sizes.

Model number	Housing Size (mm)	Peak Spatial Average SAR (W/Kg) Averaged over 1 gram	Peak Spatial Average E-field (V/m) Averaged over 2x2x2 mm ³
A2650, BCG-E8140A; A2889, BCG-E8150A; A2890, BCG-E8151A; A2891/A2892, BCG-E8152A	71.45 x 147.46	0.0000024	0.123
A2651, BCG-E8141A; A2893, BCG-E8154A; A2894, BCG-E8155A; A2895/A2896, BCG-E8156A	77.5 x 160.7	0.0000020	0.11

From the above table, we can see that housing size has very less impact on the SAR and E-field values.

The SAR plots comparison for different form factors is shown below.

Table 5. Peak Spatial Average SAR (W/Kg) plots for different housing sizes

Model number	Housing Size (mm)	Peak Spatial Average SAR (W/Kg) Averaged over 1 gram
A2650, BCG-E8140A; A2889, BCG-E8150A; A2890, BCG-E8151A; A2891/A2892, BCG-E8152A	71.45 x 147.46	
A2651, BCG-E8141A; A2893, BCG-E8154A; A2894, BCG-E8155A; A2895/A2896, BCG-E8156A	77.5 x 160.7	

The Housing size is shown to have small impact on the SAR and E-field values. It can be observed that the housing with smaller size will leak the most from the side, but the SAR numbers are still less than 0.01% of SAR limit of 1.6 W/Kg.

7 Summary

Based upon the above results, the accuracy of the SAR simulations is demonstrated by correlating H-field measurements to simulations. The validity of using this modeling and SAR computational method hence is established for iPhone models FCC IDs: BCG-E8140A, BCG-E8150A, BCG-E8151A, BCG-E8152A, BCG-E8141A, BCG-E8154A, BCG-E8155A, BCG-E8156A. Among, the exposure cases, the highest peak spatial 1-gram averaged SAR of 0.0000024 W/Kg and the highest peak spatial average E field (i.e., averaged over a cube of 2 mm x 2 mm x 2 mm) of 0.12 V/m, is observed when the battery pack and the phone are misaligned with vertical separation.

Overall, the SAR is significantly lower than the SAR limit of 1.6 W/Kg (below 0.01% of the actual SAR limit). Therefore, we respectfully request that the allowance to use of this model to demonstrate RF Exposure compliance for Apple's proposed WPT products.

Annex A: Specific information for SAR computational modelling

1) Computation Resources

The models were simulated on a 96 core CPU server with an available RAM of 4 Terabytes. Each model variation took around 12 hours to complete. Based on the simulation profile, the minimum resources needed to finish these simulations will be approximately 8 core CPU with 512 GB of RAM. Using the minimum requirements simulation will likely take more time than 12 hours.

2) Algorithm implementing and validation

This section is divided into two parts. The code performance validation provides methods to determine that the finite-element algorithm in HFSS has been implemented correctly and works accurately within the constraints due to the finite numerical accuracy. It further determines the quality of absorbing boundary conditions and certain parts of the post processing algorithms that are part of HFSS. The second part has few canonical benchmarks. All benchmarks can be compared to analytical solutions of the physical problem or its numerical representation. The methods characterize the implementation of the finite-element algorithm used by HFSS in a very general way. They are defined such that it is not possible to tune the implementation for a particular benchmark or application without improving the overall quality of the code.

2.1) Code performance validation

2.1.1) Propagation homogeneous medium

A straight rectangular waveguide with ports on both ends is well suited as a first test of an implementation of the Finite-Element Method used by HFSS. The waveguide has a width of 20 mm, a height of 10 mm and a length of 300 mm. The waveguide is filled homogeneously with a material which, in three separate simulations, shall assume the following properties:

- i. $\epsilon_r = 1$, $\sigma = 0$ S/m;
- ii. $\epsilon_r = 2$, $\sigma = 0$ S/m;
- iii. $\text{Re}(\epsilon_r) = 2$, $\sigma = 0.2$ S/m.

To verify that the mesh used by HFSS is independent of orientation, the waveguide has been rotated so that it is not parallel with any principal coordinate plane (XY, XZ, YZ). The waveguide is driven in the TE₁₀ mode at 10 GHz. Reported are the magnitudes of S₂₁ and S₁₁, as well as the values of the real and imaginary parts of the propagation constant γ . The table 1, below provides the reference values [B1], acceptable result criteria, as well as the simulated results.

Table 6: Criteria for the waveguide evaluation

$\text{Re}(\epsilon_r)$	1	2	2
σ	0	0	0.2
$ S_{21} $ reference value	1	1	8.7×10^{-5}
Criterion for $ S_{21} $	≥ 0.9999	≥ 0.9999	$\pm 5 \times 10^{-6}$
$ S_{21} $ simulated results	1	1	8.7×10^{-5}
$ S_{11} $ reference value	0	0	0
Criterion for $ S_{11} $	≤ 0.003	≤ 0.003	≤ 0.003
$ S_{11} $ simulated results	0	0	0
$\text{Re}(\gamma)$ reference value	0	0	31.17 m-1
Criterion for $\text{Re}(\gamma)$	$\pm 0.1 \text{ m-1}$	$\pm 0.1 \text{ m-1}$	$\pm 2\%$
$\text{Re}(\gamma)$ simulated results	0	0	31.17
$\text{Im}(\gamma)$ reference value	138.75 m-1	251.35 m-1	253.28 m-1
Criterion for $\text{Im}(\gamma)$	$\pm 2\%$	$\pm 2\%$	$\pm 2\%$
$\text{Im}(\gamma)$ simulated results	138.75	251.35	253.28

As is seen in the above table, HFSS easily meets the criteria for properly and accurately calculating the waveguide problem.

2.2.2) Planar dielectric boundary

In order to test the reflection of a plane wave by a dielectric boundary, a rectangular waveguide can again be used. It is well known that the TE₁₀ mode can be thought of as a superposition of two plane waves [1]. Each wave's direction of propagation makes an angle θ with the axis of the wave guide, given by

$$\cos^2\theta = 1 - (c/2af)^2 \quad (1)$$

where c is the speed of light, a is the width of the wave guide and f is the frequency. Assuming the axis of the waveguide is the Z axis and assuming the waveguide is filled with vacuum for $Z > 0$ and filled with dielectric 1 with complex relative permittivity ϵ_r for $Z < 0$, Fresnel reflection coefficients for the TE and the TM cases, defined as ratios of electric field strengths, are given by [2]

$$R^{\text{TE}} = (k_{0,z} - k_{1,z}) / (k_{0,z} + k_{1,z}) \quad (2)$$

$$R^{\text{TM}} = (\epsilon_r k_{0,z} - k_{1,z}) / (\epsilon_r k_{0,z} + k_{1,z}) \quad (3)$$

where $k_{0,z}$ and $k_{1,z}$ denote the z component of the propagation vector of the plane wave in vacuum and in the dielectric, respectively. They can be evaluated through

$$k_{0,z} = k_0 \cos\theta \quad (4)$$

$$k_{1,z} = k_0 \sqrt{(\epsilon_r - \sin^2\theta)} \quad (5)$$

Finally, ϵ_r is complex and is given by

$$\epsilon_r = \text{Re}(\epsilon_r) - j\sigma/(2\pi f\epsilon_0) \quad (6)$$

where $\text{Re}(\epsilon_r)$ denotes the real part of the relative permittivity and σ is the conductivity of the medium.

For this test, a 20 mm \times 10 mm waveguide with a length of 60 mm, as shown in Figure 1, was created. The top half was filled with vacuum and the bottom half with dielectric.

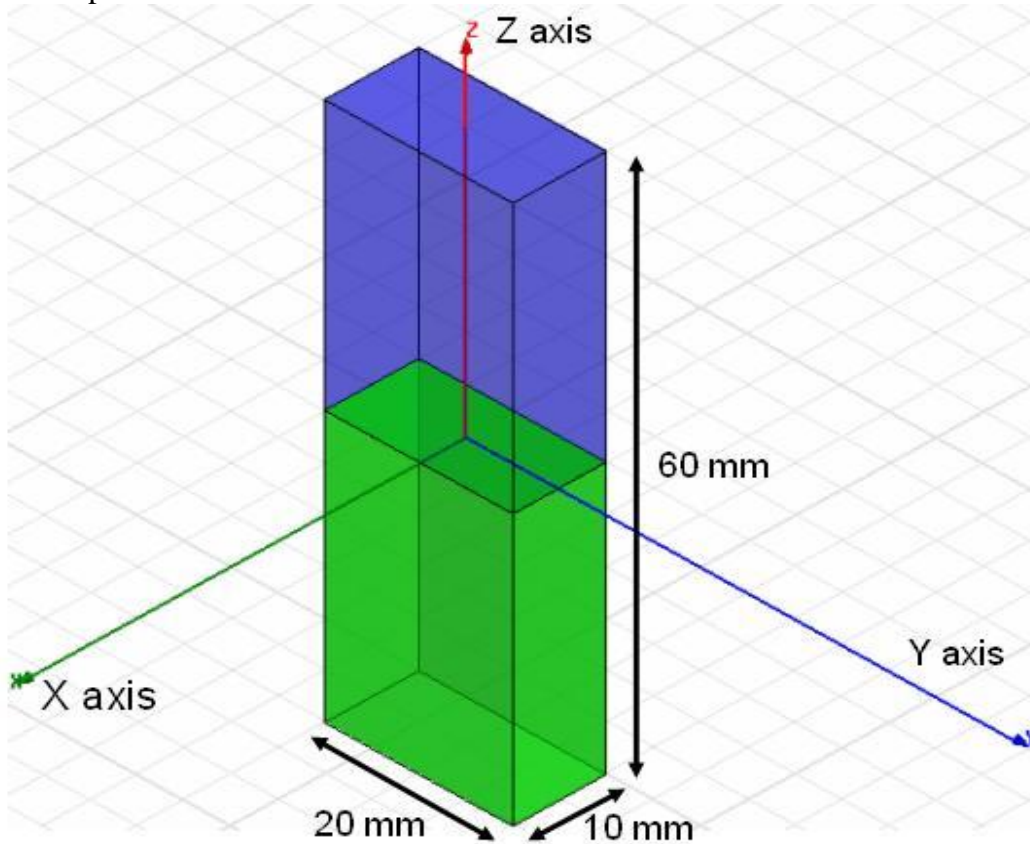


Figure 9: Waveguide filled half with vacuum and half with dielectric

In one copy of the model, all side walls were lossless metal, such that the dominant mode is the TE₁₀ mode with propagation constant 138.75 m⁻¹ at 10 GHz and represents the TE case in the reflection analysis. In the other copy of the model, the side walls that are parallel to the YZ plane were perfect magnetic conductors while the other walls were perfect electric conductors, such that the second mode (after a TEM mode which won't be used in this test) has propagation constant 138.75 m⁻¹ at 10 GHz and represents the TM case in the reflection analysis.

Before simulation, the waveguides were rotated over an arbitrary angle such that no face is parallel with any coordinate plane. The waveguides were driven at 10 GHz in the proper mode. In doing so, it is good practice to calculate all propagating modes, but the coupling between modes is expected to be negligible. Simulations were run for the cases of lossless and lossy dielectric as shown in Table 2. For the HFSS to pass the test, according to IEC 62704-1, the results need to be within 2% of the analytical values given in Table 2.

Table 7: Reflection at a dielectric interface

$\text{Re}(\epsilon_r)$	σ (S/m)	RTE	RTE- Simulated	RTM	RTM - Simulated
4	0	0.4739	0.4739	0.1763	0.1763
4	0.2	0.4755	0.4755	0.1779	0.1779
4	1	0.5105	0.5105	0.2121	0.2121

As can be seen in table 2, HFSS produces results that are identical to the analytical results.

2.2) Canonical Benchmarks

The results for few low frequency benchmarks are summarized below. These benchmarks were used to validate the accuracy of the tool at low frequencies:

2.2.1) Dipole Antenna:

The following parameter were used in the dipole antenna to resonate at 400KHz.

Dipole length: 375 meters

Feed gap: 2.5 meters

Dipole Diameter: 5 meters

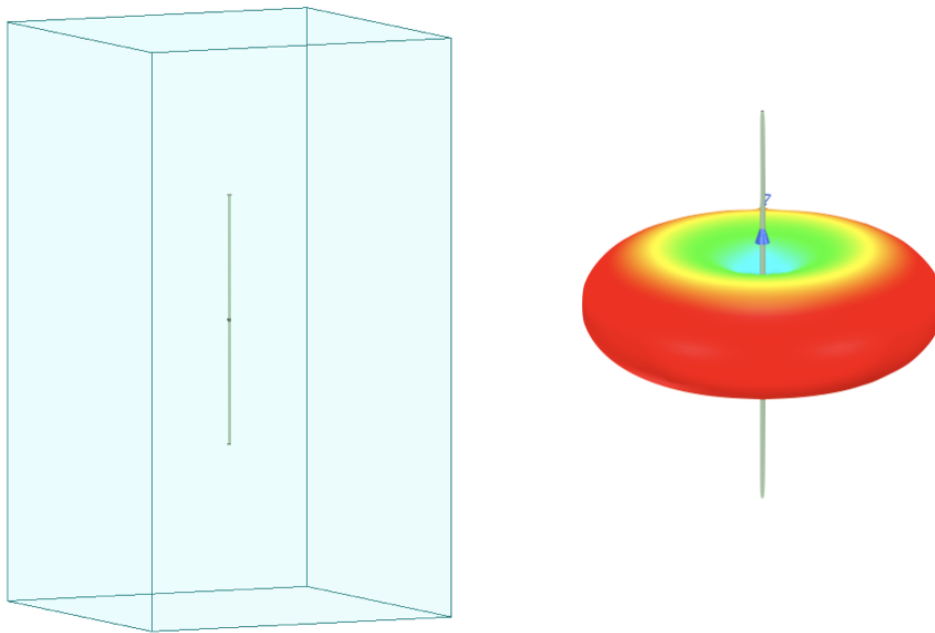


Figure 10: Dipole Antenna Model

The document IEC 62704-4 ED1 was referenced to compare the tables. Two computation methods were demonstrated as shown below to show the validity of the model.

Table 8: Simulated Dipole parameters

FEM Solver

Quantity	Simulation results	Tolerance	Satisfied?
Re(Z) at 400 KHz	94.09		
Im(Z) at 400 KHz	55.62		
Re(Z) at 320 KHz	39.26	$25\Omega < Re(Z) < 50\Omega$	Yes
Im(Z) at 320 KHz	-90.52	$-50\Omega < Im(Z) < -100\Omega$	Yes
Re(Z) at 360 KHz	59.58	$50\Omega < Re(Z) < 75\Omega$	Yes
Im(Z) at 360 KHz	-18.30	$-25\Omega < Im(Z) < 0\Omega$	Yes
Frequency for Im(Z) =0	370	$360MHz < f < 380MHz$	Yes
Maximum power budget error	0.3	$< 5\%$	Yes

MoM Solver

Quantity	Simulation results	Tolerance	Satisfied?
Re(Z) at 400 KHz	98.45		
Im(Z) at 400 KHz	53.57		
Re(Z) at 320 KHz	43.31	$25\Omega < Re(Z) < 50\Omega$	Yes
Im(Z) at 320 KHz	-90.55	$-50\Omega < Im(Z) < -100\Omega$	Yes
Re(Z) at 360 KHz	65.03	$50\Omega < Re(Z) < 75\Omega$	Yes
Im(Z) at 360 KHz	-18.59	$-25\Omega < Im(Z) < 0\Omega$	Yes
Frequency for Im(Z) =0	370	$360MHz < f < 380MHz$	Yes
Maximum power budget error	0.02	$< 5\%$	Yes

2.2.2) Toroid Inductor:

The parameters of the toroid were chosen to be

$$N = 20$$

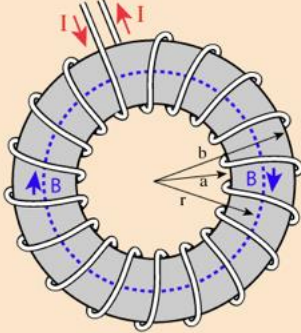
$$A = 6.35 \times 10^{-4} \text{ m}^2$$

$$R = 0.0263 \text{ m}$$

$$\mu_r = 64$$

The formula below gave an inductance of 139uH. The model created in HFSS gave an inductance of 139.9uH.

Approximate Inductance of a Toroid



Finding the [magnetic field](#) inside a [toroid](#) is a good example of the power of [Ampere's law](#). The current enclosed by the dashed line is just the number of loops times the current in each loop. Ampere's law then gives the magnetic field at the centerline of the toroid as

$$B2\pi r = \mu NI$$

$$B = \frac{\mu NI}{2\pi r}$$

The [inductance](#) can be calculated in a manner similar to that for any [coil of wire](#).

The application of [Faraday's law](#) to calculate the voltage induced in the toroid is of the form

$$\text{Emf} = -N \frac{\Delta\Phi}{\Delta t} = -NA \frac{\Delta B}{\Delta t}$$

This can be used with the magnetic field expression above to obtain an expression for the inductance.

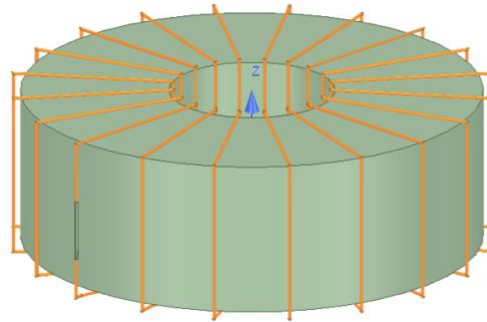
$$L \approx \frac{\mu N^2 A}{2\pi r} \quad \begin{array}{ll} A & = \text{cross-sectional area} \\ r & = \text{toroid radius to centerline} \end{array}$$


Figure 11: Toroid Model

2.2.3) Circular coil parallel to a flat, homogeneous phantom.:

The following benchmark is implemented using Equations 1-4 of the referenced Chen et al. (2014) paper and also matches Figure 6 therein scaled to 10 coil turns.

Below is the coil and phantom parameters:

Coil Diameter: 50 mm

Number of Turns: 10

RMS Current: 0.707 A (Peak current = 1 A)

Frequency: 100 kHz

Coil-to-Body Distance: 5 mm

Tissue Conductivity: 0.05 S/m

Tissue Permittivity: 1120

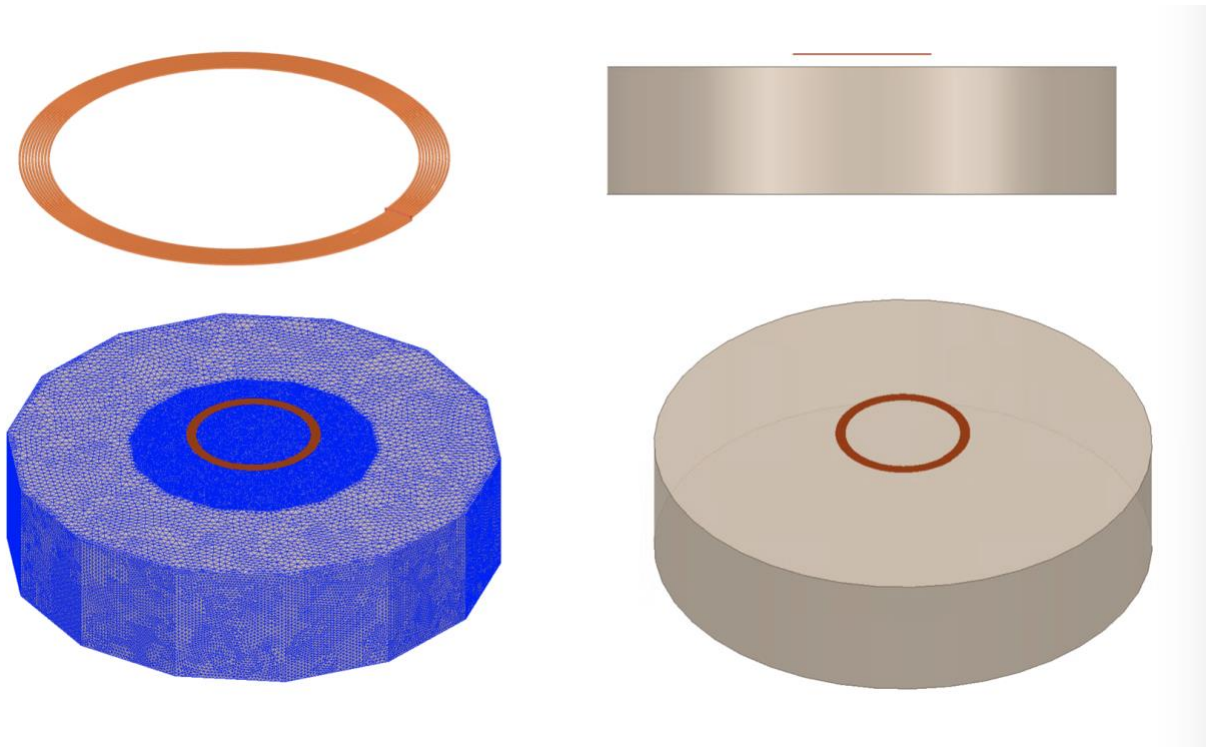


Figure 12: Current loop in front of a cuboid

The simulated spatial peak RMS electric field in tissue is 1.51 V/m compared to the analytical 1.47 V/m.

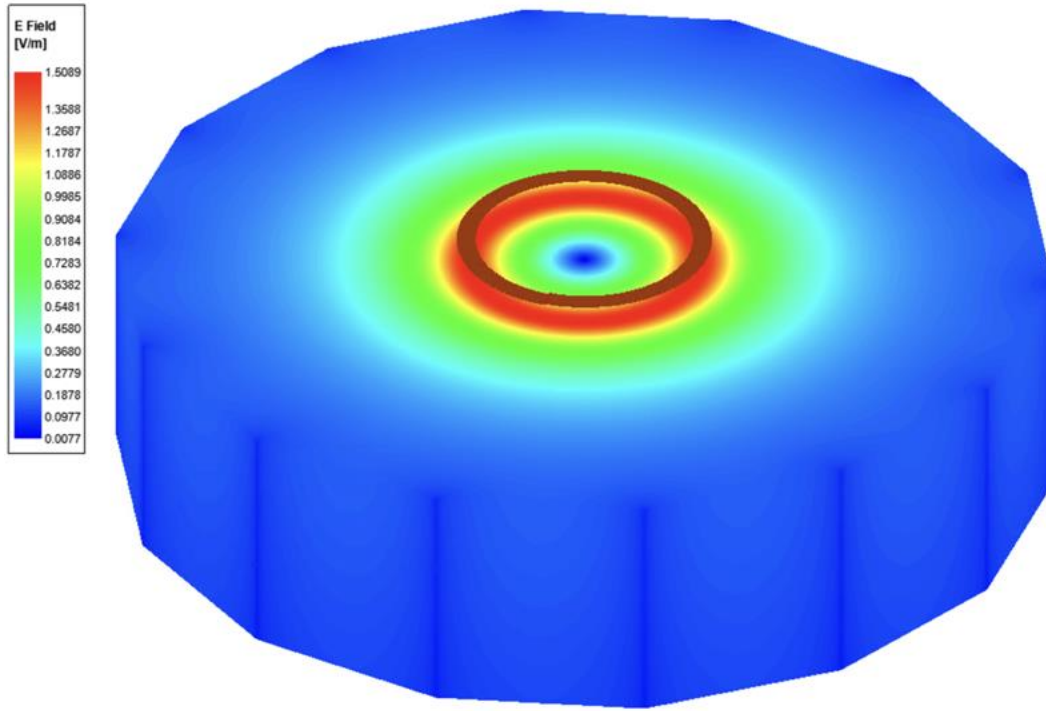


Figure 13: Current Density plot

3) Computational peak SAR from peak components & One-gram averaged SAR procedure

The calculation method for SAR follows IEEE P1528.4. Once the solver calculated the S-Parameter results, different coils can be driven and the result from the S-Parameter calculation is automatically scaled to the driving current of the coils. This result combination provides the correctly scaled power loss density in the phantom. The SAR calculation computes the local SAR first using electric field and conducting current:

$$SAR = \vec{E} \bullet \vec{J}_{conj} / (2\rho)$$

Afterwards the local SAR is averaged over a specific mass, usually 1g or 10g. As described in [IEEE P1528.4] the mass averaging is done by mapping the results to a structured hexahedral grid and afterwards the averaging scheme for FDTD per [IEEE P1528.4] is applied. The SAR calculation on the hexahedral grid is compliant with IEC 62704-1.

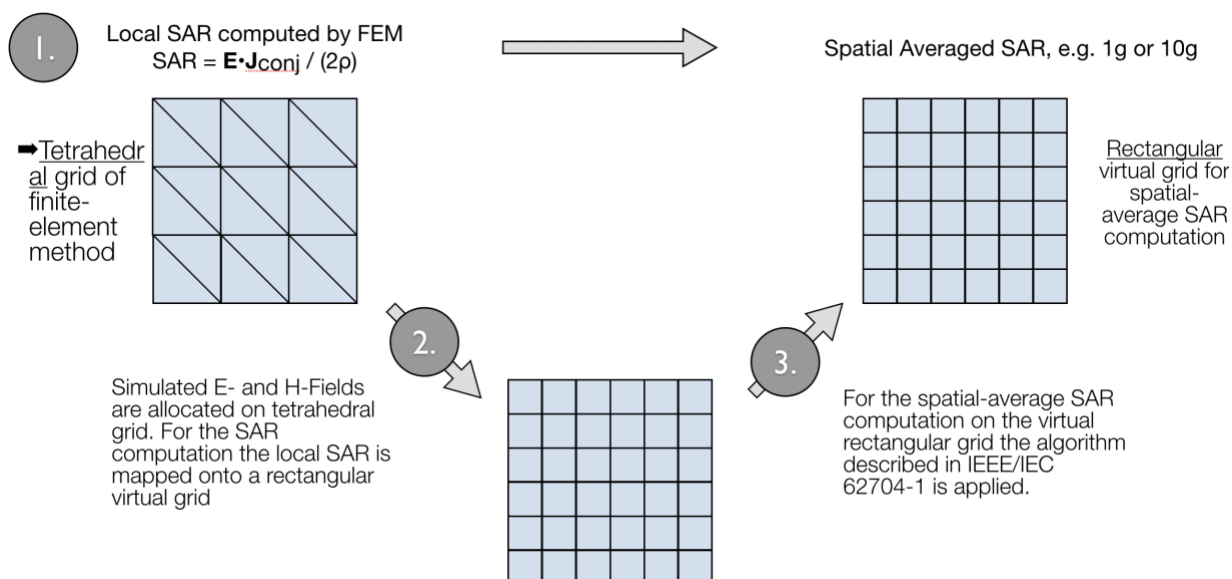


Figure 14: IEEE P1528.4 for SAR computation

4) Total Computational Uncertainty

Below is a table summarizing the budget of the uncertainty contributions of the numerical algorithm and of the rendering of the simulation setup. The table was filled using the IEC 62704-4 ED1 from 2018.

For the simulations, the extreme case where the phantom is placed directly in front of the Phone is considered.

Table 9: Budget of uncertainty contributions of the numerical algorithm (filled based on IEC 62704-4 ED1).

a	b	d	e	g
Uncertainty component	Subclause	Probability distribution	Divisor f(d, h)	Uncertainty %
Mesh resolution	7.2.3	N	1	0.06
ABC	7.2.4	N	1	0.1
Power budget	7.2.5	N	1	0.04
Convergence	7.2.6	R	1,73	0.11
Phantom dielectrics	7.2.7	R	1,73	0.004
Combined standard uncertainty ($k = 1$)				0.31

Below is a table summarizing the budget of the uncertainty of the developed model of the DUT so far. The table was filled using the IEC 62704-4 ED1 from 2018.

Table 10: Uncertainty of DUT Model

a	b	d	e	g
Uncertainty component	Subclause	Probability distribution	Divisor f(d, h)	Uncertainty %
Uncertainty of the DUT model (based on near field distribution)	7.2.2	N	1	8.6
Uncertainty of the measurement equipment and procedure	7.2.3	N	1	4
Combined standard uncertainty ($k = 1$)				12.6

The expanded ($K=2$) uncertainty results as per the IEC/IEEE 62704-1/-4 is listed in Table 7. The expanded standard uncertainty is 25.6, which is lower than the limit of 30.

Table 11: Expanded Standard Uncertainty

a	b	c	d	e	f	g	h
Uncertainty component	Sub clause	Tolerance %	Probability distribution	Divisor f(d,h)	c_i	Uncertainty %	v_i or v_{eff}
Uncertainty of the test setup with respect to simulation parameters	7.2		N	1	1	0.31	
Uncertainty of the developed numerical model of the test setup	7.3		N	1	1	12.6	
Combined standard uncertainty ($k = 1$)						12.91	
Expanded standard uncertainty ($k = 2$)						25.8	

Columns c, g and h shall be filled in based on the results of Table 5 and Table 6

NOTE 1 Column headings a to h are given for reference

NOTE 2 Abbreviation used in Table 5:

N – normal probability distribution

NOTE 3 The divisor is a function of the probability distribution and degrees of freedom (v_i and v_{eff})

NOTE 4 c_i is the sensitivity coefficient that is applied to convert the variability of the uncertainty component into a variability of SAR

The properties of the key materials of the DUT, as well as their tolerances, are listed in the following table.

Table 12: Material Properties and Tolerances

	Permittivity +/- Tolerance	Permeability +/- Tolerance	Loss Tangent +/- Tolerance	Conductivity +/- Tolerance
TX Ferrite	1	1345 +/-134	0	0
RX Ferrite	1	3300 +/-825	0	0
TX Coil	1	1	0	5.8e7 +/- 5.8e5
RX Coil	1	1	0	5.8e7 +/- 5.8e5
TX Shield	1	1	0	6.1e7 +/- 6.1e5
RX Shield	1	1	0	5.8e7 +/- 5.8e5

References:

- 1) The electrical conductivity of human cerebrospinal fluid at body temperature, S.B. Baumann ; D.R. Wozny ; S.K. Kelly ; F.M. Meno, IEEE Transactions on Biomedical Engineering (Volume: 44 , Issue: 3 , March 1997)
- 2) C.Gabriel, S.Gabriel and E.Corthout: The dielectric properties of biological tissues: I. Literature survey, Phys. Med. Biol. 41 (1996), 2231-2249.
- 3) S.Gabriel, R.W.Lau and C.Gabriel: The dielectric properties of biological tissues: II. Measurements in the frequency range 10 Hz to 20 GHz, Phys. Med. Biol. 41 (1996), 2251-2269.
- 4) S.Gabriel, R.W.Lau and C.Gabriel: The dielectric properties of biological tissues: III. Parametric models for the dielectric spectrum of tissues, Phys. Med. Biol. 41 (1996), 2271-2293.
- 5) <https://itis.swiss/virtual-population/tissue-properties/database/thermal-conductivity/>
- 6) <http://hyperphysics.phy-astr.gsu.edu/hbase/magnetic/toroid.html>
- 7) X. L. Chen et al., "Human Exposure to Close-Range Resonant Wireless Power Transfer Systems as a Function of Design Parameters," in IEEE Transactions on Electromagnetic Compatibility, vol. 56, no. 5, pp. 1027-1034, Oct. 2014.